Sensors and Actuators Reports 8 (2024) 100221

Contents lists available at ScienceDirect

Sensors and Actuators Reports

journal homepage: www.sciencedirect.com/journal/sensors-and-actuators-reports

Ultra-fast detection of pathogens and protein biomarkers using a low-cost silicon plasmonic biosensing platform

Athanasios Manolis [a,*], Christia Eleftheriou [a], Mahmoud A. Elrabiaey [a], George Tsekenis [a], Sabato D'Auria [b], Antonio Varriale [c], Alessandro Capo [c], Maria Staiano [c], Bartos Chmielak [d], Anna Lena Schall-Giesecke [d,e], Stephan Suckow [d], Dimitris Tsiokos [a]

[a] Bialoom Ltd, 72, 28th Octovriou Avenue, Office 301, Engomi, 2414 Nicosia, Cyprus
[b] Department of Biology, Agriculture and Food Science, CNR, Piazzale Aldo Moro, 7 - 00185 Rome, Italy
[c] ISA-CNR, Institute of Food Science, Via Roma 64, 83100 Avellino, Italy
[d] AMO GmbH, Advanced Microelectronic Center Aachen (AMICA), Otto-Blumenthal-Strasse 25, 52074, Aachen, Germany
[e] Chair of Electronic Components and Circuits, University of Duisburg-Essen, and Fraunhofer IMS, Duisburg, Germany

ARTICLE INFO

Keywords:
Bacteria detection
Protein detection
Silicon photonics
Plasmonic transducer
Lab on chip
Biosensor

ABSTRACT

In this paper, we report, for the first time to our knowledge, a new versatile and future proof diagnostic platform for diverse applications and heterogeneous biological targets. This platform relies on a plasmonic-augmented silicon photonic biochip to detect bacteria and protein biomarkers within minutes. To demonstrate the potential of this platform in diverse applications, we demonstrate the detection of two heterogeneous targets, the bacterium *Escherichia coli* (*E. coli*) and the molecule C-reactive protein (CRP) using a universal detection method. *E. coli* is one of the most commonly encountered bacterial pathogens involved in food monitoring, food born infections and water contamination applications, while CRP is a well-established disease severity indicator frequently used in common clinical practice. The biochip used is fully compatible with CMOS semiconductor manufacturing, while it hosts biosensors arrays for any combination of detection assays. Each biosensor exploits a 70 μm long aluminum plasmonic transducer within a silicon nitride waveguide-based Mach–Zehnder Interferometer. Each aluminum surface was silanized and biomodified with specific antibodies. Biosensing experiments revealed that CRP can be detected in diverse sample mediums, and *E. coli* detection was achieved in buffer at concentrations as low as 10 cells/ml within 13–25 min. The results are in good agreement with preceding numerical simulations. The modular nature of the reported biosensing platform makes it scalable and customizable, allowing nearly any combination of diagnostic tests targeting pathogens and proteins to be integrated on the same biochip for food quality monitoring, environmental monitoring, drug discovery and modern cell therapy manufacturing, or biomedical applications.

1. Introduction

Rapid, parallel and accurate detection of heterogeneous biochemical targets is crucial in various modern applications, such as food safety, environmental monitoring or point of care medical diagnostics. Conventional diagnostic methods and analyzers, often suffer from limitations such as long processing times, the requirement for specialized equipment and trained personnel and a lack of multi-functionality. Specifically, pathogen identification for food safety relies on time-consuming lab-based cultures or expensive molecular methods making them inappropriate for fast decision making in the field for more effective food safety control and water quality monitoring. Numerous molecular techniques, including Real-Time Polymerase Chain Reaction (RT-PCR), Loop-Mediated Isothermal Amplification (LAMP) and microarrays have emerged as alternatives to culture-based methods. While these approaches enable highly sensitive bacterial identification with faster results, they require sample amplification and use of fluorescence labels, offering also limited multiplexing capabilities (if any) at very high cost. Additionally, these technologies cannot perform protein detection which may be simultaneously required in same or different applications like medical diagnostics. These challenges underscore the urgent need for versatile, cost-effective, and scalable diagnostic

* Corresponding author.
E-mail address: amanolis@bialoom.com (A. Manolis).

https://doi.org/10.1016/j.snr.2024.100221
Received 20 March 2024; Received in revised form 28 June 2024; Accepted 2 July 2024
Available online 3 July 2024

platforms that can provide reliable and immediate detection and quantification of multiple types of analytes for numerous applications.

Up until now, electrochemical and Quartz Crystal Microbalance (QCM) biosensors have demonstrated promising results for rapid, label-free and real-time bacteria identification. For instance, *Escherichia coli* (*E. coli*) detection was achieved using an electrochemical biosensor [16,21,31], while *Salmonella typhimurium* was detected using a QCM biosensor [22,26]. However, these technologies frequently encounter a range of constraints, including limited multiplexing capabilities, high cost and, in some cases complex assays with signal amplification. Over the last decade optical biosensors and specifically silicon photonic biosensors, have been gaining attention in the field of microbiological testing. This is mainly due to their ability to offer highly sensitive analysis, miniaturization, cost-effective production and rapid, label-free real time detection. Silicon photonic biosensors have been demonstrated in bimodal interferometric and Mach–Zehnder Interferometer (MZI) schemes for simultaneous detection of bacteria down to 40 CFU/ml [2,17]. However, a scalable solution that can effectively perform label-free detection of diverse types of analytes (bacteria and proteins) addressing high-volume production needs, is still missing.

Herein, we present, for the first time, a new versatile and multi-functional diagnostic platform that relies on plasmonic-augmented silicon photonics [18] to address the growing needs of a broad spectrum of applications including food safety, water quality monitoring, drug discovery, modern cell therapy manufacturing and point-of-care diagnostics. We demonstrate a biochip capable of detecting both bacteria and protein biomarkers within minutes. As a proof-of-concept, we report the detection of *E. coli*, a commonly encountered pathogen in diverse applications, and C-reactive protein (CRP), a disease severity and inflammation indicator in medical diagnostics, using a multiplex-ready biosensing platform. The biochip is compatible with CMOS semiconductor manufacturing and can accommodate multiple heterogeneous detection assays. Each biosensor on the biochip utilizes a 70 μm long aluminum (Al) plasmonic transducer within a silicon nitride waveguide-based Mach–Zehnder Interferometer. The ultra-small footprint of the sensing transducer enables ultra-high integration density paving the way for hyperplexed assays on a single chip. For the proof-of-concept use cases, we developed an immunoassay to immobilize specific antibodies targeting direct detection of CRP and *E. coli*, on the sensing transducers. Initially, we demonstrate the biochip's efficacy in detecting *E. coli* and CRP in buffer medium. Results showed clear detection of both targets with bacteria concentrations reaching down to 10 cells/ml. In a second step, further validation of the biosensor was carried out for medical diagnostics using patient samples. CRP detection in serum was achieved for concentrations in the clinical range between 2 μg/ml and 170 μg/ml within 13 min.

2. Materials and methods

2.1. The silicon plasmonic biosensor

The proprietary plasmo-photonic biosensor chip is described in Manolis et al. [18] and conceptually depicted in Fig. 1(a). This device integrates a 70 μm long Al stripe-based plasmonic waveguide in the upper arm of a Si_3N_4-based MZI and serves as the sensing transducer by detecting local changes in the refractive index of the surrounding medium (Fig. 1(b)). Specifically, the supported Transverse Magnetic (TM) polarized plasmonic mode is fully exposed to the overlying medium and, thus, any changes in the refractive index (RI) of the applied solution result in a differential phase change in the sensing branch. Eventually, the MZI translates this phase change to a shift of the MZI resonance that is easy to interpret. In order to counter-balance the losses introduced by the plasmonic waveguide and achieve equal amplitude field interference at the interferometer output, a thermo-optically controlled Variable Optical Attenuator (VOA) is deployed in the reference photonic arm. Moreover, tuning of the resonant wavelength and sensor calibration is accomplished by a thermo-optic phase shifter in series with the VOA. Detailed design analysis, biochip fabrication and experimental characterization of the proposed biosensor can be found in [3,4,6,19]. Insets in Fig. 1(b) present schematics of captured pathogens and proteins on the Al surface.

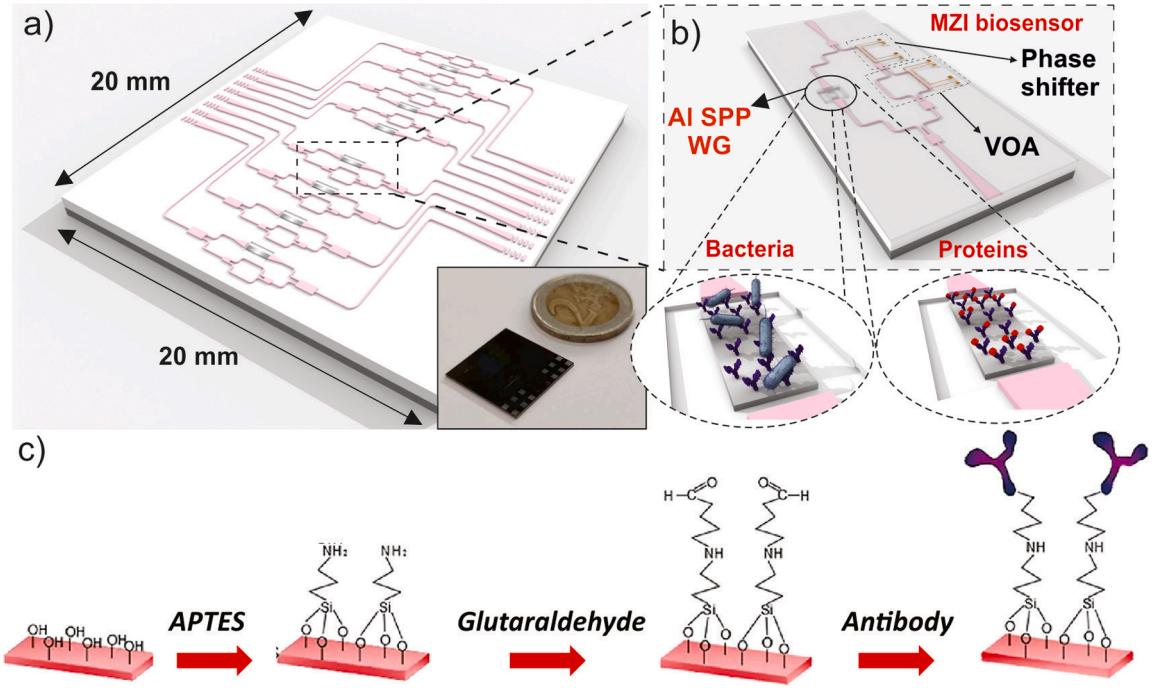

Fig. 1. (a) Conceptual schematic of current biochip (inset): photo of biochip—A two Euro coin is included for dimension comparison, and (b) Schematic of MZI biosensors layout. Insets present schematics of captured pathogens and proteins on the Al surface, (c) Schematic representation of APTES functionalization of aluminum surfaces and subsequent conjugation of antibodies with the use of the homobifunctional crosslinker glutaraldehyde.

2.2. Biochip surface functionalization and antibody immobilization

The cleaning procedure of the biochips involved successive immersion in pure acetone for 30 min, isopropanol for 10 min and driyng using N_2. Surface activation was achieved by immersing the chips in a 0.1 M HCl aqueous solution for 10 min, rinsed with deionized water, and dried using N_2. Subsequently, the chips were incubated with 5 % (3-Amino-Propyl TriethoxySilane) APTES solution in 95 % ethanol for 2 h at room temperature. The chip surfaces were then washed with 95 % ethanol aqueous solution and dried under N_2 gas flow. The chips were then cured in an oven at 110 °C for 1 h, leading to the exposure of reactive amino groups (—NH_2) on the chip surface. The amino-reactive surfaces were then treated with a 5 % v/v glutaraldehyde in Phosphate-Buffered Saline (PBS) (pH = 7.4) solution for 1 h at room temperature, rinsed with PBS and deionized water, and dried using N_2. Glutaraldehyde was used to form an aldehyde-terminated surface which allows the reaction of amine groups by the formation of imines. The sensing surfaces were then ready of antibody immobilization. This was achieved by spotting droplets of approximately 600 nL of antibody solution (Anti-CRP/*Anti-E.coli*) on each sensing area (Al plasmonic waveguides) using a pipette. The antibody solution used to spot sensing areas was prepared by diluting the stock solution (1 mg/ml) with PBS at a final concentration of 100 μg/ml. Following the antibody spotting, surfaces were incubated in humid environment for 1 h at room temperature. Significant antibody volume reduction down to picolitre range can be achieved by using commercially available automated nano-dispensing instruments (spotter), reducing the overall production costs. Finally, the chips were rinsed with PBS, blocked with 1 % Bovine Serum Albumin (BSA) in PBS solution for 1 h, and placed on the measurement setup. Fig. 1(c) shows the APTES functionalization of aluminum surfaces and the subsequent conjugation of antibodies.

2.3. Numerical simulations

A computational model was developed and used to simulate the biosensor performance for validation and optimization of both protein and bacteria binding.

2.3.1. CRP binding

Numerical simulations were conducted using Ansys-Lumerical tools [10] to simulate wavelength shift resulting from full coverage of CRP on the plasmonic waveguide. The simulation process consists of three steps. Firstly, the plasmonic waveguide's frequency-dependent properties were obtained from the eigenmode solver, including effective index (n_{eff}), loss, and group index (n_g). The plasmonic waveguide includes a silane layer of 4 nm thickness, followed by an antibody layer of 10 nm thickness on top. The RI of the silane and antibody layers were assumed to be 1.338 [9] and 1.38 RIU [23], respectively.

In the second step, the simulation was repeated with the plasmonic waveguide covered with a CRP layer above the antibody layer. The CRP layer has a RI of 1.45 [12] and a thickness of 4 nm. Once the frequency properties were calculated from the eigenmode simulations, they were incorporated into a circuit-level simulation for a more comprehensive analysis of the sensor's performance. This will determine the actual wavelength shift in response to the presence of CRP. The electric field distribution for the plasmonic mode, obtained from Eigenmode simulations, is illustrated in Fig. 2(a). The spectral responses of the sensor with and without CRP are illustrated in Fig. 2(b). According to the

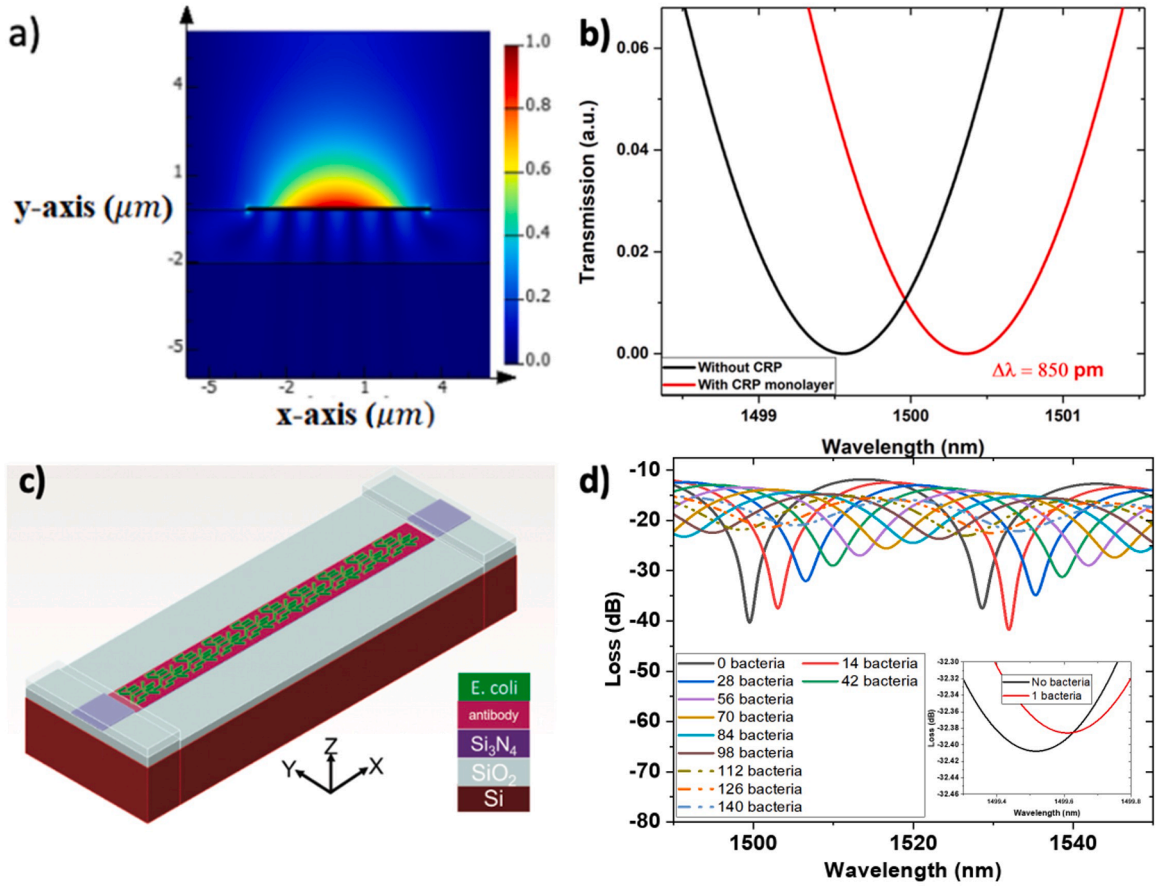

Fig. 2. (a) The field distribution for the plasmonic mode and (b) spectral response for CRP as a monolayer on the surface of the plasmonic waveguide. (c) Geometry of 3D FDTD model for the plasmonic waveguide filled with 140 bacteria, (d) spectral response for 0 to 140 bacteria bound on the plasmonic waveguide surface (inset shows the spectral response for single bacterium binding on the plasmonic waveguide surface).

circuit-level simulation, a wavelength shift ($\Delta\lambda$) of 850 pm was observed, when CRP fully covers the aluminum waveguide surface.

2.3.2. *E. coli binding*

Following the simulation results for protein binding (CRP), further simulations were conducted to calculate the wavelength shift expected from bacteria binding on the Al surface. Finite Difference Time Domain (FDTD) and circuit-level simulations were employed. The FDTD simulation domain was set with a width of 10 μm, a length of 70 μm and a height of 10 μm to simulate the full geometry of the plasmonic waveguide (Fig. 2(c)). The simulation process consisted of three steps, similar to those described for CRP simulations. Firstly, a 3D FDTD simulation was conducted to compute the phase and amplitude of the propagating plasmonic mode in the presence of silane and antibody layers on top of the plasmonic surface.

Subsequently, 3D FDTD simulation was performed including bacteria bound to the antibody layer. Lastly, the phase and amplitude of the propagating plasmonic mode, derived from the 3D FDTD simulation, were transferred to a circuit-level simulation through S-parameters to calculate the expected $\Delta\lambda$. During the 3D simulation, the *E. coli* bacteria were modeled as dielectric cylinders with a length of 2 μm and with a diameter of 500 nm. Several scenarios were examined in the simulation, including the detection of a single bacterium as well as clusters of bacteria, ranging from 14 to 140 cells (Fig. 2(d)). The goal was to compute the wavelength shift caused by the presence of different number of bacteria on the plasmonic waveguide. The circuit simulation analysis indicates a $\Delta\lambda$ of 50 pm for the detection of a single bacterium (inset of Fig. 2(d)). In a separate study, bacteria were organized into clusters, with each cluster consisting of 14 bacteria. The clusters were arranged within an area of 5 μm x 7 μm. To cover the plasmonic waveguide, a total of 10 clusters were used resulting in a total of 140 bacteria. Fig. 2(d) illustrates the sensor spectral response for different bacteria clusters, with the expected $\Delta\lambda$ ranging between 3.5 nm (14 bacteria) and 34 nm (140 bacteria). The elevated $\Delta\lambda$ values, obtained from the bacteria binding can be attributed to the optimal overlap between the propagating plasmonic mode and the captured bacteria cells. More specifically, the dimensions of *E. coli* [14,29], are comparable to the evanescent field decay length of the Al plasmonic waveguide in an aqueous environment (2 μm), leading to enhanced sensitivity for *E. coli* detection. Furthermore, through the simulation, it was observed that by placing approximately 84 bacteria (organized into 6 clusters) on the surface of the Al plasmonic waveguide, a nearly 2π phase shift can be achieved. This configuration covers approximately 50 % of the Al surface area, validating the high sensitivity credentials of the plasmonic waveguide for bacteria detection.

3. Results and discussion

3.1. CRP and E. coli detection in buffer

Bulk RI sensitivity of the plasmo-photonic biosensor was initially characterized with different PBST solutions and found equal to 1533 nm/RIU. A full analysis of the biosensor bulk RI sensitivity measurements can be found in Section S5. Following the evaluation of the bulk RI sensitivity, the plasmo-photonic biosensor was tested for the detection of CRP and *E. coli* in buffer spiked samples.

3.1.1. *CRP detection in buffer*

To demonstrate the capability of the proposed biosensor to detect protein biomarkers in buffer samples, the biosensor system was evaluated using the acute phase protein CRP. The Al surface of the plasmonic transducer was modified according to the protocols described in Section 2.2, while human anti-CRP antibodies (Invitrogen MA1-10320) were immobilized on the sensor surface as biorecognition elements. Tris-Buffered Saline with 0.1 % Tween (TBST) samples were spiked with increasing concentrations of CRP (Sigma-Aldrich C4063) in the range from 0 to 20 μg/mL. Each CRP-spiked sample was flowed through the biosensor channel for 25 min with a flow rate of 20 μl/min (II, III, IV) while TBST buffer washing steps (I) were employed before and after each CRP sample to wash the surface from unbound molecules and retain a common reference for the bulk RI medium. The sensor response was determined using the experimental setup and the algorithm explained in Section S4. The obtained biosensor response over time for the increasing CRP concentrations is presented in Fig. 3(a). During the spiked CRP samples (II, III, IV), a clear red shift of the resonance wavelength can be observed. This wavelength shift is a product of protein binding to the anti-CRP antibody and bulk RI change due to the increasing concentration of CRP in the buffer solution. When the cladding medium of the sensing transducer return to the baseline TBST buffer solution (I), a clear offset can be detected, which is the result of the CRP protein molecules specifically bound to the anti-CRP antibody on the sensor surface. The absolute wavelength shifts for each concentration are depicted in a column diagram in Fig. 3(b), indicating clear detection for all concentration, with higher concentrations resulting to larger wavelength shifts. The range of CRP concentrations tested, showed a linear concentration-dependent profile, as depicted in Fig. 3 (c), while the extracted calibration curve showing a sensitivity of $S = 50.8 \pm 4.5$ pm/μg/ml and a coefficient of determination (R^2) of the regression line greater than 98 %. Based on the signal standard deviation $\sigma = 5$ pm (Supplementary Section S5), the limit of detection was calculated according to the following formula [13]:

$$LOD = \frac{3\sigma}{S}$$

and found equal to Limit of Detection (LOD) = 0.29 μg/ml.

3.1.2. *E. coli detection in buffer*

For the detection of *E. coli* bacteria in buffer, the biosensor chip was modified with the same protocols described in Section 2.2, while *anti-E. coli* antibodies were immobilized on the surface. Anti-Ecoli production is described in Section S1 and Anti-*E. coli* to *E. coli* binding is verified by means of indirect ELISA test, explained in Section S2. For the biosensor performance evaluation in bacteria detection, an *E. coli* stock solution with concentration of 10^9 cells/ml was prepared. *E. coli* growth is described in Section S3. Inactivation of the bacteria was performed by heating the *E. coli* stock solution to 55 °C for 15 min. Salmonella samples were also prepared, in the same way, to perform control measurements and evaluate cross reactivity of the antibody with a different pathogen. Bacteria were inactivated as a safety precaution. *E. coli* samples were prepared by diluting the stock solution with PBST buffer to 4 different final concentrations (10 cells/ml, 10^2 cells/ml, 10^4 cells/ml and 10^5 cells/ml) with sample volumes of 600 μl. Furthermore, a single salmonella sample of 600 μL was prepared with a concentration of 10^5 cells/ml. Each sample was then flowed through the biosensor channel for 30 min with a flow rate of 20 μl/min (II, III, IV, V, VI) while PBST buffer washing steps(I) were employed before and after each pathogen sample to wash the surface from unbound cells and retain a common reference for the bulk RI medium. As in the case of CRP detection, the sensor response was determined using the experimental setup and the algorithm explained in Section S4. Fig. 4(a), (b) show the biosensor signal response to different *E. coli* concentrations while Fig. 4(c) depicts the selectivity test by performing a control experiment with the Salmonella sample. It is clear from the obtained sensorgrams that the sensor corresponds to the increasing *E. coli* concentrations with larger wavelength shifts. Additionally, the salmonella sample introduces a bulk RI change, due to the high concentration of bacteria included in the sample, which is removed as soon as the surface is washed with the PBST reference buffer. Fig. 4(d) presents the absolute wavelength shifts introduced by the various samples in the form of a bar diagram. The resulting wavelength shift for the non-specific sample containing *Salmonella* (control measurement) is negligible (10 pm) and at least 4 times smaller than the

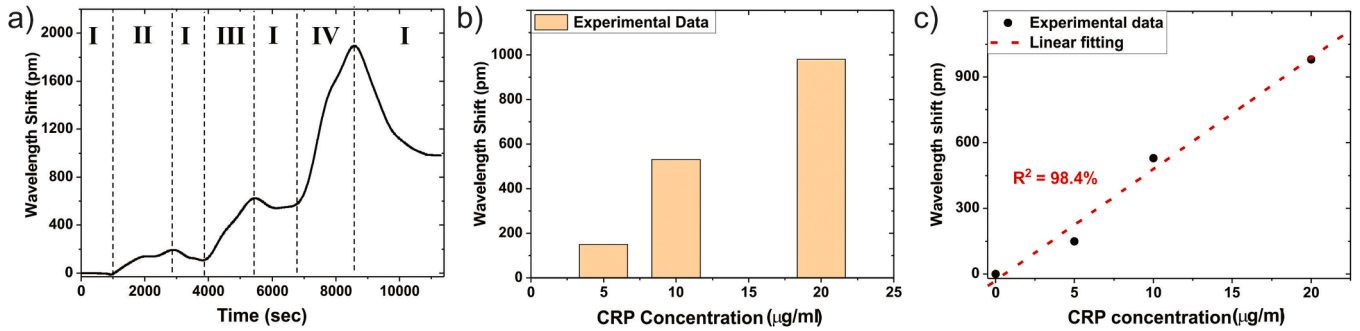

Fig. 3. (a) Real time monitoring of the wavelength shift for increasing CRP concentrations, 5 μg/ml (II), 10 μg/ml (III), 20 μg/ml (IV) in spiked buffer samples. (b) absolute wavelength shift for each CRP concentration, (c) Resonance wavelength shift as a function of CRP concentration and linear regression curve fitting the experimental results.

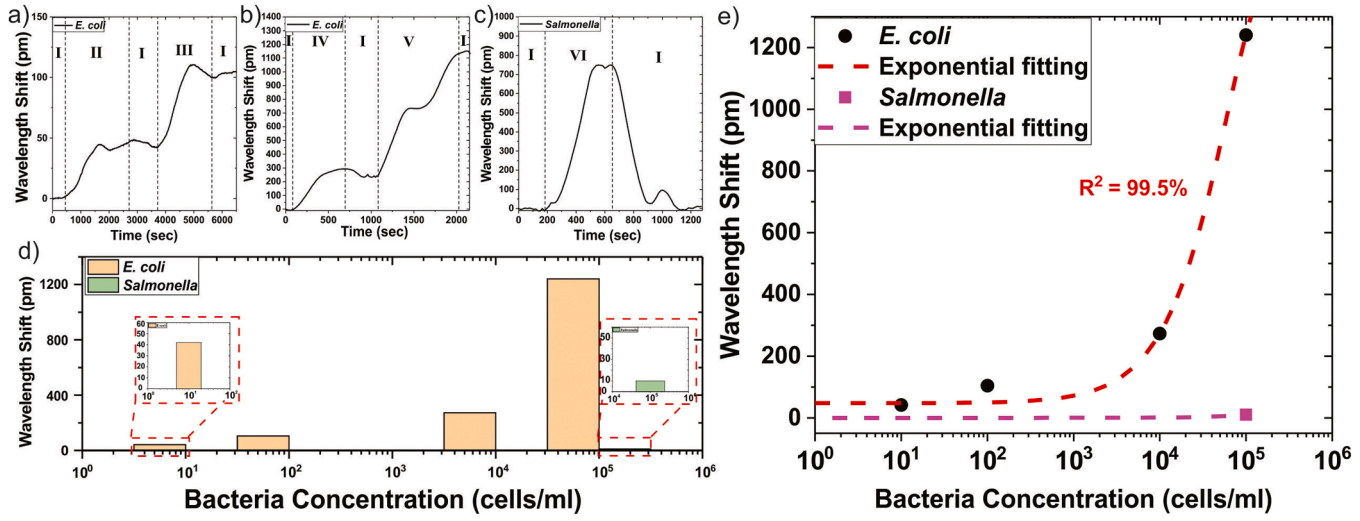

Fig. 4. (a), (b) Real time monitoring of the wavelength shift for increasing *E. coli* concentrations, 10 cells/ml (II), 10^2 cells/ml (III), 10^4 cells/ml (IV), 10^5 cells/ml (V) in buffer samples. (c) Real time monitoring of the wavelength shift for the salmonella sample (VI) (control experiment) (d) Bar diagram of the wavelength shift for each bacteria concentration. (e) Calibration curve for *E. coli* (black circles) and for non-specific bacteria Salmonella (magenta squares).

wavelength shift obtained for the lowest *E. coli* concentration of 10 cells/ml (42 pm). This may be attributed to the minimum modification of the surface that comes inherently after any sample flow over the sensing surface. Furthermore, considering the lowest *E. coli* concentration and the sample volume (600 μL), we can conclude that the actual number of bacteria detected was 6 (LOD = 10 cells/ml). Additionally, photonic numerical simulations in Section 2.3.2 dictated that the minimum expected wavelength shift for single bacterium binding is 50 pm, which closely matches the experimentally measured wavelength shift of 42 pm for the lowest *E. coli* concentration, suggesting that only 1 bacterium was attached on the Al surface. In fact, most of the bacteria flowed far from the sensing surface in the sample volume that did not interact with the biosensor surface. This mainly stems from the fluidic dynamics, allowing most of the bacteria to escape, indicating that the proposed platform LOD can be further improved by optimizing the mass transport of bacteria in the microfluidic channel. Consequently, a calibration curve (Fig. 4(e)) was generated after analyzing the obtained data for the bacterial concentrations under test.

3.2. Biosensor validation with patient samples

To showcase the assay's potential when applied in clinical environments, we assessed the feasibility of testing blood serum samples. Performance evaluation of the biosensor was conducted using pre-measured patient serum samples collected from our external partners StArtBio, an in-vitro diagnostic services center in Athens, Greece [8] ("https://startbiology.com/),") and diluted 1:5 with TBST (20 % serum). CRP concentration quantification by ELISA was previously performed on the serum samples under test. The sample data is summarized in Table 1.

Each patient's serum sample was diluted in TBST buffer to achieve a 20 % serum (1:5 dilution) resulting into the final concentrations of 1.2 μg/ml, 3 μg/ml, 15 μg/ml and 34 μg/ml. For the validation experiments, 5 independent sensors were modified with the biofunctionalization protocol described in Section 2.2, and anti-CRP antibodies (previously used for the measurements in Section 3.1.1) were immobilized on the sensor surface. Subsequently, the serum samples were flowed over the sensor surface for 13 min with a flow rate of 20 μl/min. A few washing steps of TBST buffer were employed before and after each serum sample to wash away any unbound molecules. Fig. 5(a) shows a representative sensorgram. The sensorgram starts with a steep increase of the

Table 1
Serum samples data summary.

Sample ID	CRP concentration in whole serum (μg/ml)	CRP concentration in 20 % serum (μg/ml)
S1	0 (control)	0 (control)
S2	6	1.2
S3	15	3
S4	45	15
S5	170	34

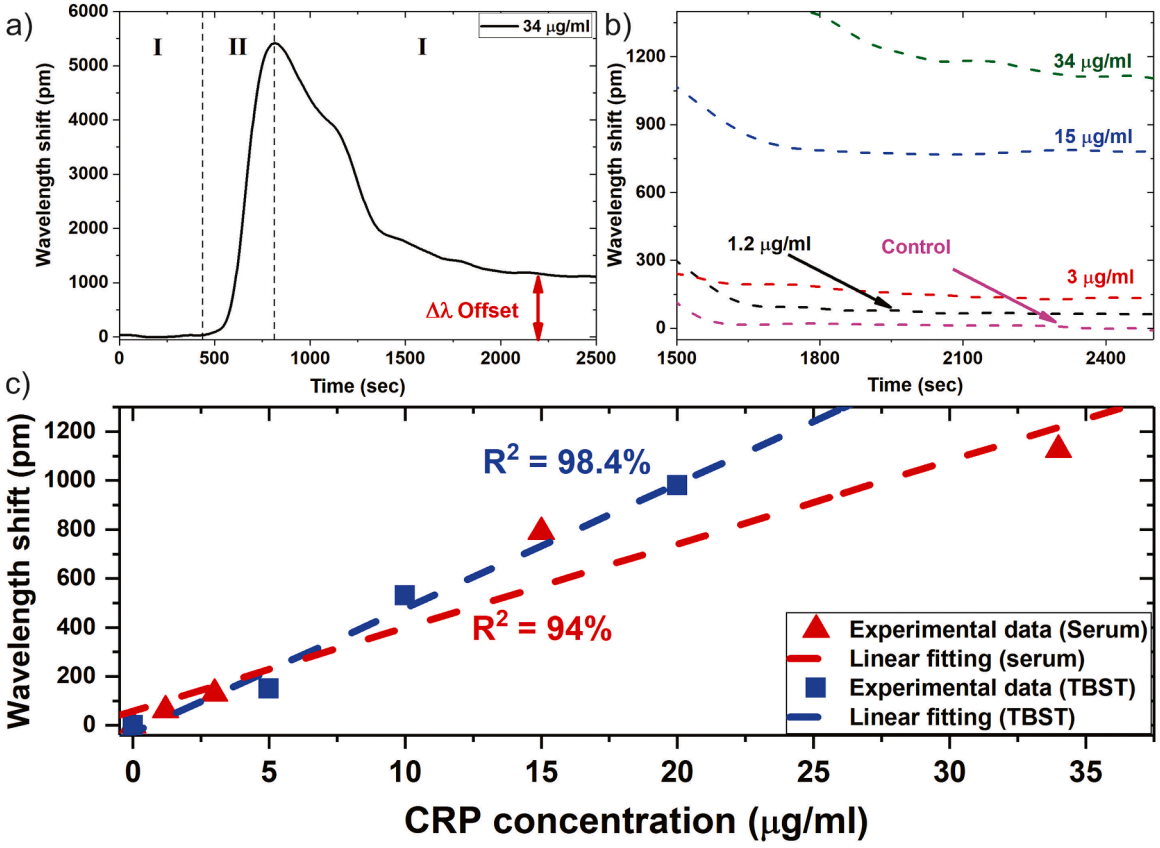

Fig. 5. (a) Real-time sensorgram For 34 μg/ml CRP concentration in serum (1:5), (b) Δλ offset for different CRP concentrations in diluted serum (1:5), (c) Calibration curve for CRP detection in diluted serum (1:5).

wavelength shift (II), resulting from the bulk effect coming from the serum medium (i.e. RI increases due to the presence of serum compared to the smaller RI of the TBST buffer), which is stabilized after the TBST washing step (I), resulting in the net signal (offset) coming from the interaction of the antigen (CRP) with the antibodies (anti-CRP) immobilized on biosensor surface.

Fig. 5(b) presents the net signal change for the various analyte concentrations after the serum samples have passed through the sensor. Furthermore, a control experiment was conducted, using CRP-free serum samples. Similarly, to the detection of CRP in buffer, the net wavelength shift reveals a linear dependency on the CRP concentration (Fig. 5(c)), resulting in a sensitivity of $S = 37 \pm 5.2$ pm/μg/ml and coefficient of determination (R^2) of 94 %. The LOD was calculated equal to 0.4 μg/ml based on the formula, provided in Section 3.1.1, using the sensitivity derived from the calibration curve in Fig. 5(c), and the standard deviation of the signal (σ). Given that the dilution factor is 1:5 the LOD in the undiluted serum sample is 5×0.4 μg/ml $= 2$ μg/ml.

4. Discussion

The successful demonstration of our silicon plasmonic biosensing platform paves the way for multi-analyte diagnostic solutions in various applications, such as food safety, environmental monitoring, drug discovery and modern cell therapy manufacturing or point of care medical diagnostics. To give a perspective on the features and benefits of the proposed biosensor platform, a detailed comparison between the performance characteristics of various photonic integrated biosensors employing silicon photonic and plasmonic sensing transducers in different configurations found in the literature is presented in Table 2.

Au-based structures have been reported for Lens-free Interferometric Microscopy (LIM) relying on nanoplasmonics combined with custom bioprinted microarrays. This approach enables direct label-free bacteria (*E. coli*) quantification allowing for low LOD values in blood plasma, however noble metal materials and accurate fabrication control requirements, hinder their mass production and hence their cost-effectiveness. On the other hand, integrated biosensors relying on silicon photonic platforms have been reported in the literature in many different configurations, including Ring Resonators (RRs), Mach Zehnder and Bi-Modal interferometers, with the potential to realize mass-produced chips at a low cost. Interferometric layouts, although demonstrating good sensitivities for protein (0.8 μg/ml) and for bacteria detection (40 CFU/ml), detection of heterogeneous analytes is still missing while many of those approaches use complex detection assays for signal amplification [2]. Additionally, sensing transducer length of several millimeters is required in most cases [13,17,30], limiting sensor integration density potential, increasing antibody volume requirements and therefore increasing manufacturing cost. RR biosensors have been reported showcasing small footprints with multiplexing capabilities. Finally, one approach using RR sensors demonstrate successful detection of proteins and bacteria achieving LOD value of 0.2 μg/ml for proteins and 10^5 CFU/ml for bacteria with limited dynamic range and no validation with patient samples [25].

In this work, our proof-of-concept experiment demonstrates the viability of the proposed biosensing platform to successfully detect and quantify heterogeneous targets at low cost with high multiplexing potential driven by the unique footprint and performance credentials of the Al plasmonic transducer. Finally, there is room for sensitivity improvement by (a) increasing the MZI FSR (Evangelia [3]), (b) by optimizing the microfluidic channel design to enhance mass transport dynamics as reported in Lynn et al. [15] and (c) by exploiting more effective detection assays [28] (i.e. oriented immobilization of capturing antibodies).

Table 2
Comparison with biosensors reported in the literature, employing silicon photonic and plasmonic transducers (*upper boundaries of the dynamic range are limited by the availability of samples at the time of experiments and may not constitute a hard limit of the maximum detectable concentration).

Ref.	Configuration	CMOS	Target (s)	LOD (experimental)	LOD (theoretical)	Dynamic range	Assay amplification	Sensing length (μm)	Medium	Time to result (min)
[7]	Plasmonic	×	Bacteria	400 cells/ml	NA	400–10^5 cells/ml	NO	1750	Plasma	30
[17]	Bimodal WG	✓	Bacteria	4 CFU/ml	NA	4–10^4 CFU/ml	NO	15,000	Ascitic fluid	15
[30]	MZI	✓	Proteins	1 μg/ml	NA	1–25 μg/ml	NO	10,000	Buffer	20
[2]	MZI	✓	Bacteria	40–110 CFU/ml	NA	40– 10^6 CFU/ml	YES	600	Water/ Milk	15
[13]	MZI	✓	Proteins	0.8 μg/ml	NA	0.8–40 μg/ml	NO	1800	Buffer	20
[25]	RR	✓	Bacteria, antibodies	10^5 CFU/ml, 0.2 μg/ml	NA	10^5–10^9 CFU/ml, 0.2–0.4 μg/ml	NO	100 (Diameter)	Buffer	60, 10
[11]	RR	✓	Bacteria	10^8 CFU/ml	NA	10^8 CFU/ml - NA	YES	100 (Diameter)	Buffer	15
[1]	RR	✓	Proteins	0.2 μg/ml	NA	0.2–10 μg/ml	YES	200 (Diameter)	Plasma	3–15
This work	Silicon plasmonic MZI	✓	Bacteria, Proteins	10 cells/ml (*E. coli* in buffer), 0.29 μg/ml (CRP in buffer), 2 μg/ml (CRP in serum)	1 cell/ml	*10–10^5 cells/ml, *2–170 μg/ml	NO	70	Buffer, Serum	13–25

5. Conclusions

We introduced a new CMOS-compatible plasmonic-augmented silicon photonic biosensor platform for label-free detection of bacteria and protein analytes within minutes in diverse sample mediums (buffer, serum) for different applications. Experimental results revealed that the plasmo-photonic biosensor was able to detect *E. coli* bacteria at a concentration as low as 10 cells/ml in buffer while sensor validation with patient serum samples demonstrated detection of CRP in the in the range 2–170 μg/ml in serum, employing a label-free immunoassay. The high-sensitivity credentials offered by the proposed biosensing platform against bacteria detection, are attributed to the optimum overlap between the target analyte (bacterium) and the uniquely exposed optical mode of the proposed plasmonic waveguide. Each detection was performed within 13–25 min, with no requirement of pretreatment or signal amplification, achieving CRP detection with concentrations within the clinical range for healthy individuals and patients with inflammation or infection [5,20,24,27].

In conclusion, the plasmo-photonic biosensor performance has been successfully evaluated, demonstrating rapid, label-free and cost-effective detection of *E. coli* and CRP using a future proof multiplexed-ready biosensing chip compatible with very large-scale chip fabrication in commercial semiconductor facilities. The modular nature of the reported biosensing platform makes it scalable and customizable enabling the parallel detection of nearly any possible combination of microbiological and biochemical tests on the same biochip. The proposed technology may address the needs of faster diagnosis in a wide range of modern application, from PoC medical diagnostics to drug discovery and modern cell therapy manufacturing to food safety and environmental monitoring.

CRediT authorship contribution statement

Athanasios Manolis: Writing – review & editing, Writing – original draft, Visualization, Validation, Supervision, Methodology, Investigation, Formal analysis, Data curation, Conceptualization. **Christia Eleftheriou:** Writing – review & editing, Writing – original draft, Methodology, Data curation. **Mahmoud A. Elrabiaey:** Writing – review & editing, Writing – original draft, Visualization, Software, Investigation. **George Tsekenis:** Writing – original draft, Supervision, Investigation, Conceptualization. **Sabato D'Auria:** Writing – review & editing, Supervision, Investigation. **Antonio Varriale:** Writing – review & editing, Writing – original draft, Resources, Methodology, Investigation. **Alessandro Capo:** Writing – review & editing, Writing – original draft, Resources, Investigation, Data curation. **Maria Staiano:** Resources, Investigation. **Bartos Chmielak:** Resources, Investigation. **Anna Lena Schall-Giesecke:** Investigation. **Stephan Suckow:** Writing – review & editing, Writing – original draft, Resources, Investigation. **Dimitris Tsiokos:** Writing – review & editing, Writing – original draft, Supervision, Project administration, Methodology, Investigation, Funding acquisition, Formal analysis, Conceptualization.

Declaration of competing interest

The authors declare that they have no known competing financial interests or personal relationships that could have appeared to influence the work reported in this paper.

Data availability

The data that has been used is confidential.

Acknowledgments

This work has been funded by the European Union's Horizon 2020

Research and Innovation Programme under grant agreement no. 101007448 (GRACED). Bialoom acknowledges support of Startbio (https://startbiology.com) for providing patient samples for the system validation. Bialoom acknowledges Dr. Stefan Schrittwieser and Dr. Rainer Hainberger from the Austrian Institute of Technology (AIT) for providing the microfluidic structures.

Supplementary materials

Supplementary material associated with this article can be found, in the online version, at doi:10.1016/j.snr.2024.100221.

References

[1] E. Aljohani, S. Gundavarapu, C.A. Chapman, A.P. Arroyo, G. Chen, C.-C. Lin, A. Romig, K. Preston, A. Vinitsky, A. Gonzales, E. Hsu, J. Cobb, Y. Rybakova, M. Dubrovsky, D. Vermeulen, Silicon photonics system for low-cost rapid quantification of biomarkers in blood, in: 2023 IEEE Silicon Photonics Conference (SiPhotonics). Presented at the 2023 IEEE Silicon Photonics Conference (SiPhotonics), 2023, pp. 1–2, https://doi.org/10.1109/SiPhotonics55903.2023.10141929.

[2] M. Angelopoulou, P. Petrou, K. Misiakos, I. Raptis, S. Kakabakos, Simultaneous detection of *Salmonella typhimurium* and *Escherichia coli* O157:H7 in drinking water and milk with Mach–Zehnder interferometers monolithically integrated on silicon chips, Biosensors 12 (2022) 507, https://doi.org/10.3390/bios12070507.

[3] E. Chatzianagnostou, D. Ketzaki, G. Dabos, D. Tsiokos, J.-C. Weeber, A. Miliou, Design and optimization of open-cladded plasmonic waveguides for CMOS integration on Si_3N_4 platform, Plasmonics. 14 (2019) 823–838, https://doi.org/10.1007/s11468-018-0863-7.

[4] Evangelia Chatzianagnostou, A. Manolis, G. Dabos, D. Ketzaki, A. Miliou, N. Pleros, L. Markey, J.-C. Weeber, A. Dereux, B. Chmielak, A.-L. Giesecke, C. Porschatis, P. J. Cegielski, D. Tsiokos, Scaling the sensitivity of integrated plasmo-photonic interferometric sensors, ACS Photonics 6 (2019) 1664–1673, https://doi.org/10.1021/acsphotonics.8b01683.

[5] B. Clyne, J.S. Olshaker, The C-reactive protein 1, J. Emerg. Med. 17 (1999) 1019–1025, https://doi.org/10.1016/S0736-4679(99)00135-3.

[6] G. Dabos, A. Manolis, D. Tsiokos, D. Ketzaki, E. Chatzianagnostou, L. Markey, D. Rusakov, J.-C. Weeber, A. Dereux, A.-L. Giesecke, C. Porschatis, T. Wahlbrink, B. Chmielak, N. Pleros, Aluminum plasmonic waveguides co-integrated with Si_3N_4 photonics using CMOS processes, Sci. Rep. 8 (2018) 13380, https://doi.org/10.1038/s41598-018-31736-4.

[7] P. Dey, N. Fabri-Faja, O. Calvo-Lozano, R.A. Terborg, A. Belushkin, F. Yesilkoy, A. Fàbrega, J.C. Ruiz-Rodriguez, R. Ferrer, J.J. González-López, M.C. Estévez, H. Altug, V. Pruneri, L.M. Lechuga, Label-free bacteria quantification in blood plasma by a bioprinted microarray based interferometric point-of-care device, ACS Sens. 4 (2019) 52–60, https://doi.org/10.1021/acssensors.8b00789.

[8] https://startbiology.com/.

[9] https://www.gelest.com/wp-content/uploads/Hydrophobicity-Hydrophilicity_and_Silane_Surface_Modification.pdf.

[10] https://www.lumerical.com/.

[11] S. Janz, D.-X. Xu, M. Vachon, N. Sabourin, P. Cheben, H. McIntosh, H. Ding, S. Wang, J.H. Schmid, A. Delâge, J. Lapointe, A. Densmore, R. Ma, W. Sinclair, S. M. Logan, R. MacKenzie, Q.Y. Liu, D. Zhang, G. Lopinski, O. Mozenson, M. Gilmour, H. Tabor, Photonic wire biosensor microarray chip and instrumentation with application to serotyping of *Escherichia coli* isolates, Opt. Express 21 (2013) 4623–4637, https://doi.org/10.1364/OE.21.004623.

[12] S. Kastner, P. Pritzke, A. Csáki, W. Fritzsche, The effect of layer thickness and immobilization chemistry on the detection of CRP in LSPR assays, Sci. Rep. 12 (2022) 836, https://doi.org/10.1038/s41598-022-04824-9.

[13] D. Kohler, G. Schindler, L. Hahn, J. Milvich, A. Hofmann, K. Länge, W. Freude, C. Koos, Biophotonic sensors with integrated Si_3N_4-organic hybrid (SiNOH) lasers for point-of-care diagnostics, Light Sci. Appl. 10 (2021) 64, https://doi.org/10.1038/s41377-021-00486-w.

[14] P.Y. Liu, L.K. Chin, W. Ser, T.C. Ayi, P.H. Yap, T. Bourouina, Y. Leprince-Wang, Real-time measurement of single bacterium's refractive index using optofluidic immersion refractometry, Procedia Eng. 87 (2014) 356–359, https://doi.org/10.1016/j.proeng.2014.11.743. EUROSENSORS 2014, the 28th European Conference on Solid-State Transducers.

[15] N.S. Lynn, H. Šípová, P. Adam, J. Homola, Enhancement of affinity-based biosensors: effect of sensing chamber geometry on sensitivity, Lab. Chip 13 (2013) 1413–1421, https://doi.org/10.1039/C2LC41184A.

[16] R. Maalouf, C. Fournier-Wirth, J. Coste, H. Chebib, Y. Saïkali, O. Vittori, A. Errachid, J.-P. Cloarec, C. Martelet, N. Jaffrezic-Renault, Label-free detection of bacteria by electrochemical impedance spectroscopy: comparison to surface Plasmon resonance, Anal. Chem. 79 (2007) 4879–4886, https://doi.org/10.1021/ac070085n.

[17] J. Maldonado, A.B. González-Guerrero, C. Domínguez, L.M. Lechuga, Label-free bimodal waveguide immunosensor for rapid diagnosis of bacterial infections in cirrhotic patients, Biosens. Bioelectron. 85 (2016) 310–316, https://doi.org/10.1016/j.bios.2016.04.095.

[18] A. Manolis, E. Chatzianagnostou, G. Dabos, D. Ketzaki, B. Chmielak, A.L. Giesecke, C. Porschatis, P.J. Cegielski, S. Suckow, L. Markey, J.-C. Weeber, A. Dereux, S. Schrittwieser, R. Heer, N. Pleros, D. Tsiokos, Ultra-sensitive refractive index sensor using CMOS plasmonic transducers on silicon photonic interferometric platform, Opt. Express 28 (2020) 20992–21001, https://doi.org/10.1364/OE.383435.

[19] A. Manolis, E. Chatzianagnostou, G. Dabos, D. Ketzaki, D. Tsiokos, B. Chmielak, S. Suckow, A.L. Giesecke, C. Porschatis, P.J. Cegielski, L. Markey, J.-C. Weeber, A. Dereux, N. Pleros, Bringing plasmonics into CMOS Photonic foundries: aluminum plasmonics on Si_3N_4 for biosensing applications, J. Lightwave Technol. 37 (2019) 5516–5524.

[20] D. Martens, P. Ramirez-Priego, M.S. Murib, A.A. Elamin, A.B. Gonzalez-Guerrero, M. Stehr, F. Jonas, B. Anton, N. Hlawatsch, P. Soetaert, R. Vos, A. Stassen, S. Severi, W.V. Roy, R. Bockstaele, H. Becker, M. Singh, L.M. Lechuga, P. Bienstman, A low-cost integrated biosensing platform based on SiN nanophotonics for biomarker detection in urine, Anal. Methods 10 (2018) 3066–3073, https://doi.org/10.1039/C8AY00666K.

[21] Y. Mei, C. He, W. Zeng, Y. Luo, C. Liu, M. Yang, Y. Kuang, X. Lin, Q. Huang, Electrochemical biosensors for foodborne pathogens detection based on carbon nanomaterials: recent advances and challenges, Food Bioprocess Technol. 15 (2022) 498–513, https://doi.org/10.1007/s11947-022-02759-7.

[22] H.J. Min, H.A. Mina, A.J. Deering, J.P. Robinson, E. Bae, Detection of *Salmonella typhimurium* with gold nanoparticles using quartz crystal microbalance biosensor, Sensors 22 (2022) 8928, https://doi.org/10.3390/s22228928.

[23] M.J. Pollitt, G. Buckton, R. Piper, S. Brocchini, Measuring antibody coatings on gold nanoparticles by optical spectroscopy, RSC Adv. 5 (2015) 24521–24527, https://doi.org/10.1039/C4RA15661G.

[24] P. Póvoa, L. Coelho, E. Almeida, A. Fernandes, R. Mealha, P. Moreira, H. Sabino, C-reactive protein as a marker of infection in critically ill patients, Clin. Microbiol. Infect. 11 (2005) 101–108, https://doi.org/10.1111/j.1469-0691.2004.01044.x.

[25] A. Ramachandran, S. Wang, J. Clarke, S.J. Ja, D. Goad, L. Wald, E.M. Flood, E. Knobbe, J.V. Hryniewicz, S.T. Chu, D. Gill, W. Chen, O. King, B.E. Little, A universal biosensing platform based on optical micro-ring resonators, Biosens. Bioelectron. 23 (2008) 939–944, https://doi.org/10.1016/j.bios.2007.09.007.

[26] F. Salam, Y. Uludag, I.E. Tothill, Real-time and sensitive detection of *Salmonella typhimurium* using an automated quartz crystal microbalance (QCM) instrument with nanoparticles amplification, Talanta 115 (2013) 761–767, https://doi.org/10.1016/j.talanta.2013.06.034.

[27] M. Soler, M.-C. Estevez, M. Alvarez, M.A. Otte, B. Sepulveda, L.M. Lechuga, Direct detection of protein biomarkers in human fluids using site-specific antibody immobilization strategies, Sensors 14 (2014) 2239–2258, https://doi.org/10.3390/s140202239.

[28] M. Soler, L.M. Lechuga, Biochemistry strategies for label-free optical sensor biofunctionalization: advances towards real applicability, Anal. Bioanal. Chem. 414 (2022) 5071–5085, https://doi.org/10.1007/s00216-021-03751-4.

[29] S.A. Taya, D.N. Alhamss, I. Colak, S.K. Patel, Sensitivity enhancement of an optical sensor based on a binary photonic crystal for the detection of *Escherichia coli* by controlling the central wavelength and the angle of incidence, Opt. Quantum Electron. 54 (2022) 127, https://doi.org/10.1007/s11082-022-03511-3.

[30] F. Vogelbacher, T. Kothe, P. Muellner, E. Melnik, M. Sagmeister, J. Kraft, R. Hainberger, Waveguide Mach–Zehnder biosensor with laser diode pumped integrated single-mode silicon nitride organic hybrid solid-state laser, Biosens. Bioelectron. 197 (2022) 113816, https://doi.org/10.1016/j.bios.2021.113816.

[31] M. Xu, R. Wang, Y. Li, An electrochemical biosensor for rapid detection of *E. coli* O157:H7 with highly efficient bi-functional glucose oxidase-polydopamine nanocomposites and Prussian blue modified screen-printed interdigitated electrodes, Analyst 141 (2016) 5441–5449, https://doi.org/10.1039/C6AN00873A.